Changes in velocity distribution produced by paddlewheels in algae raceway ponds

Mahmoud Abbaszadeh[a,b,*], Sergio Maldonado[b], Gustavo de Almeida[b]

[a] *Department of Civil and Environmental Engineering, Imperial College London, SW7 2AZ, UK*

[b] *Faculty of Engineering and Physical Sciences, University of Southampton, Southampton SO17 1BJ, UK*

Abstract

Open raceway ponds (RWPs) are widely used in large-scale algae production. To improve the performance of these systems, it is crucial to understand the flow structure throughout the ponds. Computational fluid dynamics (CFD) simulations have been widely used to study the flow field in RWPs. However, such studies typically require assumptions about the distribution of velocities at the inlet boundary of the domain (which is usually taken as the cross-section a short distance downstream from the paddlewheel). In this study, laboratory measurements were carried out to study the flow structure in the vicinity of a paddlewheel in a raceway pond model. Results showed that the paddlewheel may induce complex changes to the distribution of depth-average velocities, including the complex inversion of the velocity gradient across the channel. The measured non-uniform distribution of velocities was then used as the boundary condition of a CFD simulation to understand the effects of common assumptions on the accuracy of CFD simulations of flows in RWPs. Furthermore, observations in a field (full-scale) installation corroborated that the presence of a paddlewheel significantly affects the velocity distribution in its vicinity, further strengthening the argument that such changes to the flow should not be disregarded in numerical simulations of RWPs.

*Corresponding author

Email address: m.abbaszadeh@imperial.ac.uk, abbaszadeh.mahmoud@gmail.com (Mahmoud Abbaszadeh)

Keywords: Velocity inversion, Raceway ponds, PIV, CFD, paddlewheel

1. Introduction

The cultivation of microalgae has received increased attention in the past decades. Microalgae are used in several applications, such as in cosmetics, pharmaceuticals, and nutritional products [1, 2]. In addition, the possibility of producing biofuel from microalgae has also been the object of intense research [3, 4, 5, 6]. Recent attention has also been given to the use of microalgae to capture atmospheric carbon [7, 8, 9].

Owing to their low construction and operational costs [10, 11], open raceway ponds (RWPs) have become the most popular choice of bioreactor for the cultivation of microalgae at large scale. RWPs are typically artificial ponds where a paddlewheel is used to recirculate the water, which promotes mixing and contributes to algal growth (see Figure 1). Mixing plays a central role in the growth of algae by preventing them from settling down to the bottom, eliminating thermal stratification, increasing the diffusion of nutrients and gases, and ensuring appropriate algal exposure to light. Computational Fluid Dynamics (CFD) is widely used to understand turbulent mixing and the complex hydrodynamics of RWPs, [12, 13, 14, 15]. CFD simulations allow us to assess the effects of different design and operational parameters on the hydrodynamic performance of RWPs in an economic manner compared to physical modeling.

One of the difficulties in simulating the hydrodynamics of RWPs via CFD is the inclusion of a rotating paddlewheel. Common methods to simulate the effects of the paddlewheel on the flow are Dynamic Mesh (DM) [16, 17] and Inlet Velocity (IV) [18, 19]. In the DM method, the rotation of the paddlewheel is simulated, and the transfer of momentum from the blades to the fluid is modelled through a rotating mesh [13, 19]. This method provides predictions of the pond's velocity field without the need for assumptions about the boundary conditions to be made. However, the significant computational cost associated with it often poses a barrier to its application. To mitigate the high computational

cost associated with the dynamic mesh simulation, other modelling techniques have been typically adopted. For example, in the IV method, the paddlewheel is not simulated, and the inlet velocity distribution (commonly assumed to be uniformly distributed) is prescribed at the inlet boundary of the computational domain (typically a channel cross-section downstream of the paddlewheel) [20]. Another alternative is to model the transfer of momentum from the blades to the flow by a momentum source in the governing equations [21, 22, 23]. Several studies have utilised the IV method and constant momentum source as alternatives to the paddlewheel in RWPs. For example, Liffman et al. [23] modelled various raceway bend configurations in order to reduce energy loss and eliminate stagnation regions, potentially enhancing algae productivity in RWPs. They used a constant momentum source with the source strength ($1\,\mathrm{kg\,m^{-2}\,s^{-2}}$) for a volume engulfing the full depth and width of the pond and extending a distance of 0.5 m along the straight channel. In another study, Lima et al. [21] assessed the hydrodynamic performance of standard raceway designs, focusing on geometry and operational conditions. They used a localised momentum source in a zone which covered the whole cross-section of the pond and spanned over a length of 0.5 m. Prussi et al. [24] analysed the mixing of algae in straight and bend sections of a $500\,\mathrm{m^2}$ RWP, using the IV method and imposing a uniform flow velocity of $0.2\,\mathrm{m\,s^{-1}}$ in the inlet boundary. Zhang et al. [25] modelled RWP incorporating flow deflectors and wing baffles, aiming to minimise dead zones and enhance the flashing light effect. They replaced the paddlewheel with a constant inlet velocity of $0.3\,\mathrm{m\,s^{-1}}$. This is despite previous CFD simulations suggesting that the velocity distribution downstream from the paddlewheel is highly non-uniform [26]. More recently, Teshome [20] investigated the hydrodynamics of a RWP both experimentally and numerically. For numerical modeling, both DM and IV (uniform velocity at the inlet) methods were utilised and the results were compared with experimental data. A good agreement was shown between the vertical velocity profiles obtained by the DM method and the experimental data downstream and in close proximity to the paddlewheel, but as expected, the IV method did not produce an accurate prediction of the vertical velocity profile in

that region. Due to the computational cost of the DM method (six weeks for a 200 s simulation) Teshome [20] took an intermediate approach to enhance the IV method. In this approach, a non-uniform velocity profile along the depth given by experimental data or the DM method was prescribed as the inlet boundary condition for the IV method. Despite the fact that the updated non-uniform velocity (vertical) profile for the IV method gave a relatively good prediction of the flow field, it did not take into account the non-uniformity across the width of the channel.

The objective of this paper is to conduct a detailed investigation of the velocity distribution in the vicinity of paddlewheels used in RWPs, and to compare laboratory measurements against the results of CFD simulations performed using different approaches to model the effects of the paddlewheel (uniform IV and momentum source). To this end, Particle Image Velocimetry (PIV) was employed in a physical model of a RWP to measure twelve vertical profiles of the streamwise velocity per cross-section, at eleven cross-sections distributed throughout the pond (i.e. a total of 132 velocity profiles). The velocity profiles measured downstream of the paddlewheel displayed a counterintuitive non-uniform distribution of the depth-averaged velocity across the channel. These measurements were then used as the inlet boundary condition for the CFD IV method. The results of simulations performed with the IV method with uniform inlet velocity and the measured (laterally non-uniform) inlet velocity were compared against the velocity measurements undertaken at other cross-sections along the pond. In addition, velocity measurements were undertaken in the vicinity of a paddlewheel in a full-scale 110 m long RWP, which also confirmed the role of paddlewheels in substantially modifying the distribution of flow velocities.

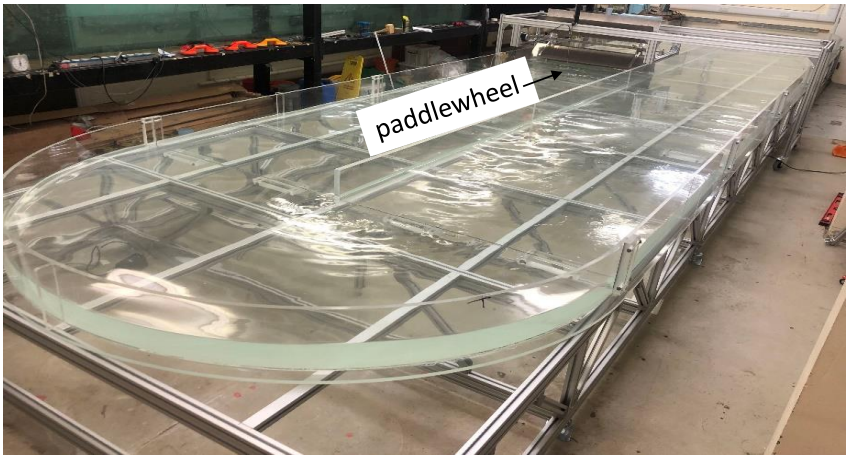

Figure 1: Physical model of the RWP. The length and width of each straight section are 10 m and 1.22 m, respectively, and the radius of the bends is 1.235 m. The water depth in the pond is 10 cm.

2. Experimental set-up and methods

2.1. Raceway pond

The physical model of the RWP is illustrated in Figure 1. The length and width of each straight section are 10 m and 1.22 m, respectively, and the radius of the bends is 1.235 m. The water depth in the pond is 10 cm and the flow is subcritical (Froude number, Fr < 1). The whole RWP pond (walls and bed) is made of acrylic to enable full optical access from the sides and from below. The paddlewheel is located in the middle of one of the straight sections and is driven by an electrical motor, which was set to produce an angular velocity of 10 rpm. The gaps between the paddlewheel and the model's bottom and sidewalls are 2 cm and 3.5 cm, respectively. To ensure steady-state conditions are reached, the pond is run for at least 10 min before any measurements are undertaken.

2.2. Experimental method

Measurement of the flow velocity was conducted by means of Particle Image Velocimetry (PIV). The flow was seeded with spherical polyamide particles with

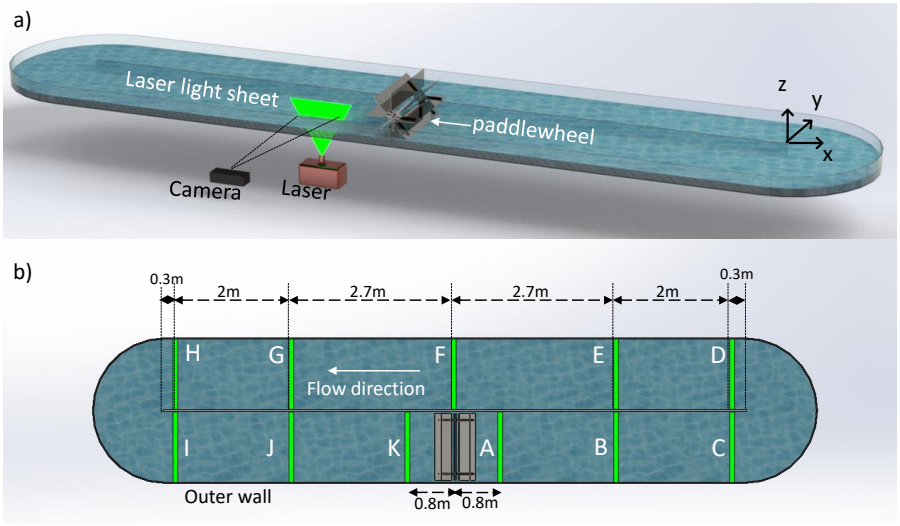

Figure 2: a) Position of the laser and camera with respect to the pond, b) Location of the cross-sections (A to K) where measurements were conducted.

an average diameter of 55 µm and density of 1.016 g/cm^3. A double-pulsed laser (300 W) at 808 nm was used for illumination. The pairs of images were recorded at the frame rate of 15 Hz by a 12-bit 1920 x 1080 pixels CCD camera with a 50 mm f1.4 Nikon lens. The time interval between two images making a pair was 200 µs. In each measurement, 7,000 pairs of frames were recorded. Frames were analysed using a grid refining scheme whereby the interrogation windows were refined sequentially from 96×96 to 32×32 pixels. This improves the dynamic spatial range (DSR) without losing the correlation due to the large displacements within the flow[27]. In each refinement step, 50% overlap for the interrogation windows was considered. Finally, to remove spurious values from the obtained velocity vectors, a normalised median test with a threshold of 3 was employed [27].

As illustrated in Figure 2.a, the laser sheet expands in the streamwise-vertical direction (i.e. the xz plane, where x and z are the streamwise and vertical coordinates, respectively). Flow measurements were conducted at eleven different cross-sections (A to K in Figure 2.b). At each cross-section, images were

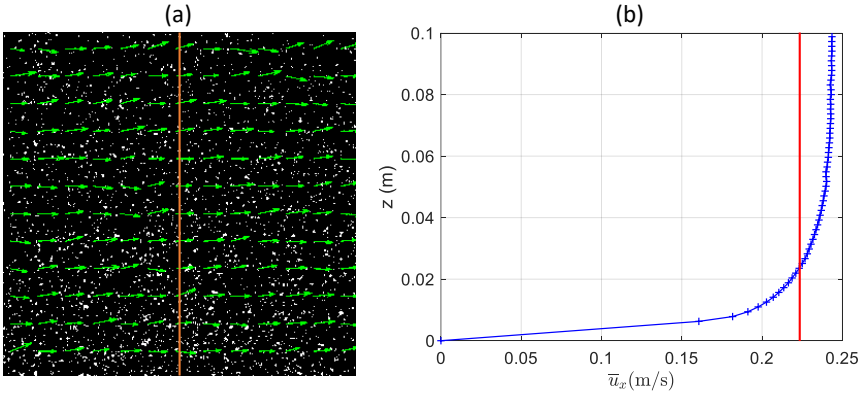

Figure 3: a) Raw image from PIV with velocity vectors superimposed, corresponding to cross-section B; b) Streamwise velocity profile (blue line) corresponding to the vertical line shown in (a) as well as its depth-averaged value (red line). Depth-averaged velocities are reported in Figure 5.

recorded at twelve planes in the spanwise (y) direction. All planes are positioned at distances ranging from 4 to 114 cm from the outer wall, with increments of 10 cm. After the measurement and in each plane at every cross-section, velocity fields are obtained that allow us to perform relevant analysis. For example, Figure 3 shows the conversion of PIV images to velocity profiles. In Figure 3.a, the raw PIV image is superimposed with the velocity vectors recorded at cross-section B, 104 cm away from the external wall. Figure 3.b illustrates the streamwise velocity profile derived from these velocity vectors, along with the resultant depth-averaged velocity; the distribution of the latter across the pond is our main target, as detailed in Section 3.1.

2.3. Numerical simulation

Three-dimensional numerical simulations of the RWP were conducted with the use of the open source code, OpenFOAM [28]. The fluid motion for incompressible, steady state, and turbulent flow conditions is modelled by the continuity and Reynolds-averaged Navier-Stokes (RANS) equations; namely:

$$\nabla \cdot (\rho \overline{\mathbf{u}}) = 0 \tag{1}$$

$$\nabla \cdot (\rho \overline{\mathbf{u}}\ \overline{\mathbf{u}}) = -\nabla \overline{p} + \{\nabla \cdot (\overline{\tau} - \tau^R)\} + \mathbf{S}, \tag{2}$$

where $\mathbf{u} = \overline{\mathbf{u}} + \mathbf{u}'$ is the instantaneous velocity vector (with the overbar and prime symbols denoting time-averaged quantities and their fluctuations, respectively, as per the Reynolds decomposition underpinning the RANS equations), ρ is the density of the fluid, $p = \overline{p} + p'$ is the instantaneous pressure, $\overline{\tau}$ and τ^R are the viscous and Reynolds stress tensors, respectively, and $\mathbf{S}$ is the momentum source. Based on the Boussinesq hypothesis [29], τ^R can be expressed as a linear function of the mean velocity gradient, such that:

$$\tau^R = -\rho\overline{\mathbf{u}'\mathbf{u}'} = \mu_t\{\nabla\overline{\mathbf{u}} + (\nabla\overline{\mathbf{u}})^T\} - \frac{2}{3}[\rho k + \mu_t(\nabla \cdot \overline{\mathbf{u}})]\mathbf{I}, \tag{3}$$

where μ_t is the eddy viscosity, k is the turbulent kinetic energy, $\mathbf{I}$ is the identity matrix, and $\nabla\overline{\mathbf{u}} + \nabla\overline{\mathbf{u}}^T$ is the strain rate tensor. Different turbulence models have been developed to compute μ_t. In this paper, the $k-\epsilon$ model was adopted, in which the turbulent kinetic energy, k, and the dissipation rate, ϵ, are calculated by solving transport equations for k and ϵ. After calculating k and ϵ, the eddy viscosity μ_t is determined by:

$$\mu_t = C_\mu \frac{\rho k^2}{\epsilon}, \tag{4}$$

where C_μ is typically taken as 0.09 [30]. By plugging (4) back into the (3) and (2), we can predict the evolution of the mean flow velocity.

2.3.1. Modelling treatment of the paddlewheel

Two alternative methods are available for simulating the paddlewheel; namely, the IV and the momentum source methods. The boundaries of the simulation domain for the IV method are illustrated in Figure 4. In this method, the boundaries of the domain are located $\pm$ 0.35 m upstream and downstream from the paddlewheel axis (outlet and inlet, respectively). At the inlet, both uniform and non-uniform velocity distributions are considered. For the non-uniform distribution, we use the flow velocity obtained from our measurements at the inlet

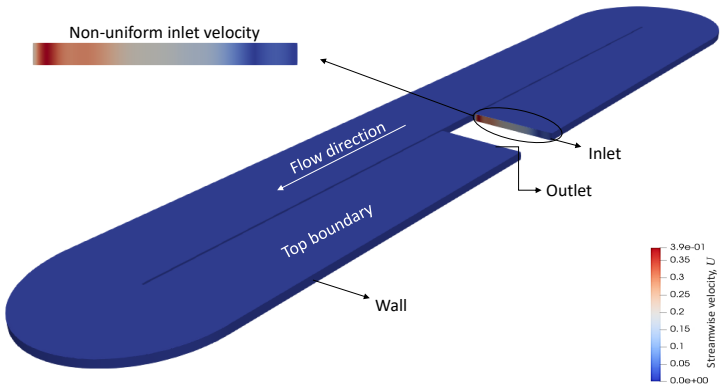

Figure 4: Simulation domain for the IV method. The non-uniform inlet velocity is displayed in the top left.

boundary to model the effect of the paddlewheel on the flow (see the inset of Figure 4). In the uniform distribution, we consider the average of the non-uniform velocity distribution as the velocity magnitude at the inlet. Other than the velocity distribution at the inlet, the remaining boundary conditions for the uniform and non-uniform IV methods remain the same. The pressure gradient at this boundary is set to zero. At the outlet, the velocity is set such that its gradient is zero, except for negative flux where this boundary condition switches to zero fixed value. At the top boundary, the slip condition and zero gradients are set for the velocity and pressure, respectively. At the wall boundary, the standard no-slip condition is defined for the velocity and the zero gradient is used for the pressure.

The constant momentum source method does not make use of inlet or outlet boundaries. Instead, the flow domain matches the physical domain, and the transfer of momentum from the blades of the paddlewheel to the flow is modelled through the source term in Eq. 2. This source is applied only to a region of the computational domain in the vicinity of the paddlewheel (specifically, to a volume spanning the whole depth and width of the flow, and 0.7 m along the longitudinal direction). In this method, the top and wall boundary conditions are the same as those used for the IV method described above.

Table 1: Grid convergence test results for four different numbers of cells.

Number of cells (million)	RMS of TKE $\times 10^{-4}$(m^2/s^2)	Relative difference (%)	RMS of velocity magnitude (m/s)	Relative difference (%)
5.4	5.16	5	0.1586	3.3
11.9	5.42	0.9	0.1640	0.11
21.7	5.47	0.4	0.1642	0.10
33.9	5.49	-	0.1640	-

2.3.2. Grid convergence test

Unstructured hexahedral cells were used to discretise the flow domain. A grid convergence analysis was done by doubling the number of cells and monitoring the root mean square (RMS) of the turbulent kinetic energy (TKE) and the velocity magnitude in the entire pond. TKE represents the energy associated with the turbulent eddies and is defined as the sum of the average of the fluctuating components of the velocity squared, and it is given by:

$$\mathrm{TKE} = \frac{1}{2}(\overline{u'^2} + \overline{v'^2} + \overline{w'^2}) \tag{5}$$

where $\overline{u'^2}$, $\overline{v'^2}$, and $\overline{w'^2}$ represent the mean of the fluctuations in the velocity (squared) components in the x, y, and z directions, respectively. The results in Table 1 show that the relative difference in the RMS of TKE and velocity magnitude is of the order of 0.1% when the number of the cells was increased from 21.7 to 33.9 million cells. Thus, 21.7 million cells were used in this study. The average characteristic length, corresponding to the final cell count of 21.7 million cells, is 10^{-2}m.

2.4. Field measurements

To further investigate the effect of paddlewheels on the distribution of flow velocities under different conditions and to shed some light on potential effects arising from scale, imperfections in construction in the real-world (i.e. not laboratory), and the location of the paddlewheel, measurements have been undertaken also at a full-scale installation in Morocco. The field prototype is 110 m long, and each section is roughly 4.5 m wide (free surface width) and

0.4 m deep (small variations are present throughout the RWP due to the construction method employed). Incidentally, this approximately represents a scale factor (relative to the laboratory model described in this paper) of 1:4 for the lateral and vertical dimensions (but not for the longitudinal dimension, which is $\sim 1 : 8.8$). However, strictly speaking, the laboratory model cannot be regarded as a scale model of this particular installation because of other differences; e.g. the cross-section is trapezoidal and the geometry is less regular in the field installation, and neither the roughness nor the flow conditions were scaled to match the prototype's conditions. Also, in this installation the paddlewheel is positioned downstream of one of the bend (the paddlewheel axis is positioned 1.5 m downstream from the bends), as opposed to the position used in the model. Acoustic Doppler Velocimetry was employed to measure vertical profile distributions of the transverse and streamwise components of velocity along two cross-sections, located 1.5 m upstream and 2.0 m downstream of the axis of the paddlewheel. A total of 10 measurement points were taken at different distances from the bottom at each vertical. The duration of measurements at each location was 90 s.

3. Results & Discussion

This section presents the results from the velocity measurements undertaken in the scale model. These measurements are then utilised to investigate how assumptions usually adopted to model the paddlewheel (e.g. uniform inlet velocity and momentum source) may affect the results of CFD simulations. Furthermore, measurements on a field installation are also reported, confirming that the paddlewheel has a strong effect on the structure of the approach flow, even when the position of the paddlewheel is changed along the RWP.

3.1. Measurements

The depth-averaged streamwise velocity (U), displayed in Figure 5, shows a general increasing trend in cross-sections A to C (i.e. highest velocities near the

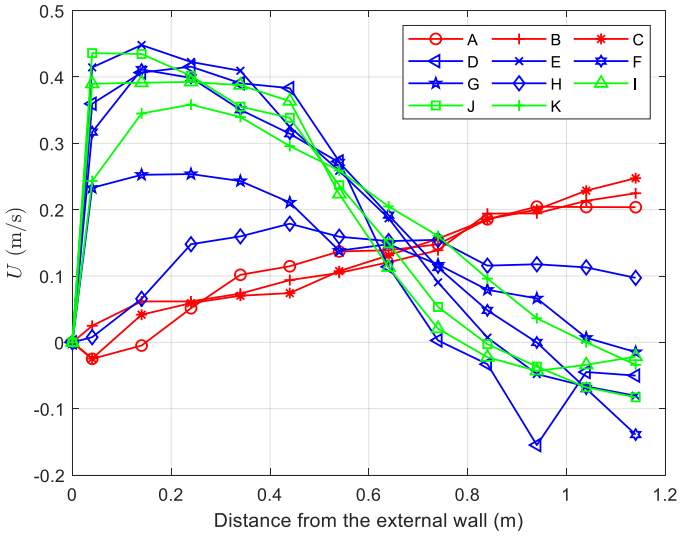

Figure 5: Depth-averaged streamwise velocity (U) against distance from the external wall for the eleven cross-sections shown in Figure 2.

central divider) and decreasing in the other cross-sections (i.e. highest velocities near the external wall of the RWP). The wake produced downstream of the first bend as a result of flow separation near the central divider is clearly observed by the velocity distribution in sections D and E. This region is also characterised by a highly unsteady flow due to the shedding of large eddies, and low mean velocities, and is usually referred to as the dead flow area. The lateral gradient in the depth-averaged streamwise flow velocity gradually decreases until the flow reaches cross-section H, where the velocity distribution across the channel is nearly uniform. A similar flow pattern is observed downstream of the second bend (i.e., sections I to K), with the flow approaching the paddlewheel with a strong transverse gradient in depth-averaged streamwise velocity. The comparison of velocity distributions at sections K and A (upstream and downstream of the paddlewheel, respectively) is particularly interesting and has been largely overlooked in the literature [20, 24, 25]. Namely, our results show that flow approaches the paddlewheel with a negative lateral gradient (i.e. highest velocities near the external wall), while downstream from the paddlewheel the gradient is

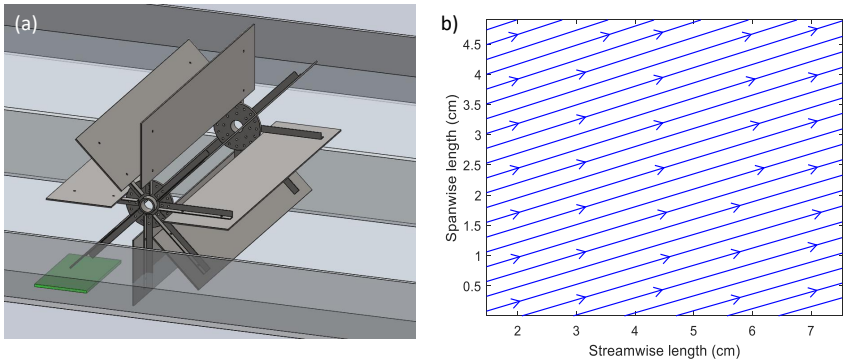

Figure 6: a) The location of the laser sheet under the paddlewheel. It spans from the outer wall to 35 cm from the outer wall. b) Streamlines between 30-35 cm from the outer wall.

inverted and the highest velocities are observed near the central divider. The inversion of the velocity distribution can be hypothetically explained as follows. Because of the strong lateral gradient in the depth-averaged streamwise velocity, the relative velocity between the flow and the blades of the paddlewheel changes substantially across the channel. This means that the flow is strongly decelerated near the external wall, producing a lateral pressure gradient, which in turn produces a spanwise flow acceleration. As a result, the depth-averaged streamwise flow velocity downstream of the paddlewheel near the central divider is higher than the velocity near the outer wall.

To further investigate the above hypothesis, we provide a more detailed visualisation of the flow in the vicinity of the paddlewheel (15 cm upstream from the axis), by examining the streamlines in the xy plane. To this end, the laser plane was shone horizontally across the pond while a camera was positioned vertically underneath the RWP (which is everywhere transparent). The laser sheet spanned from the outer wall up to a distance of 35 cm from the wall (as illustrated in Figure6.a), and was set at a height of 5 cm from the bottom. A measurement was taken at a distance from the outer wall, spanned from 30 cm to 35 cm away (see Figure 6.b). The streamlines clearly indicate that the flow deviates towards the center as it approaches the paddlewheel, providing further

evidence to support the aforementioned hypothesis.

3.2. Simulations

The observation of the radical change in the distribution of velocity by the paddlehweel has important implications for CFD simulations of RWPs. As previously discussed, the majority of existing studies of flow in RWPs modelled the effects of the paddlewheel by either a uniform IV boundary condition or a momentum source. This section examines how these modelling choices may affect the overall model predictions of flow in RWPs. To this end, the results of three simulations are compared. The first simulation uses the observed non-uniform distribution of velocities as the inlet boundary condition (i.e. our measurements at cross-section A). The effectiveness of this method was validated by comparing CFD results with PIV measurements. Figure 7 shows three examples of this validation for cross-sections C, F and I. The figure shows that the depth-averaged velocity (which is made dimensionless in Figure 7 by the maximum value of the streamwise velocity, U_{max}, at each section) predicted by the CFD simulations using the measured non-uniform IV approach closely matches the PIV results in all three cross-sections. Nevertheless, when employing the uniform IV method and the constant momentum source, a discrepancy between the depth-averaged velocity in cross-section C and the PIV results is clearly observed. Cross-sections F and I, which are further away from the boundary condition, displayed a closer match between the uniform IV method, constant momentum source, and the PIV outcomes. This outcome highlights that using a uniform IV approach and a constant momentum source primarily influences the flow field downstream of the paddlewheel.

To further illustrate this, the velocity contours for the non-uniform and uniform IV boundary conditions and the momentum source methods are presented in Figure 8. This figure shows that the influence of the modelling choice is most pronounced in the region of flow downstream of the paddlewheel. Flow between the paddlewheel and the first bend displays a distribution of velocity that is almost uniform in Figure 8.a (uniform IV), while the velocities display

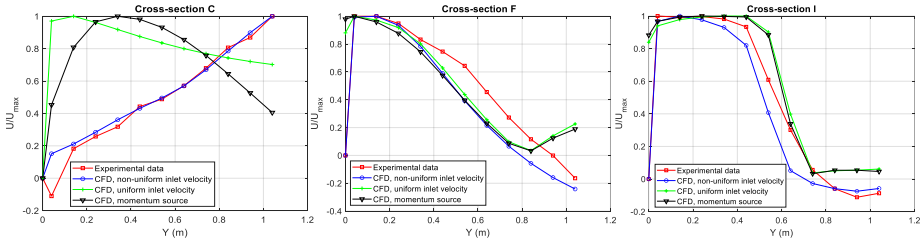

Figure 7: Validation and comparisons of the normalised depth-averaged velocity (U/U_{max}) derived by CFD against the PIV data for cross-sections C, F and I. U is the depth-averaged streamwise velocity and U_{max} is the maximum value observed in the cross-section.

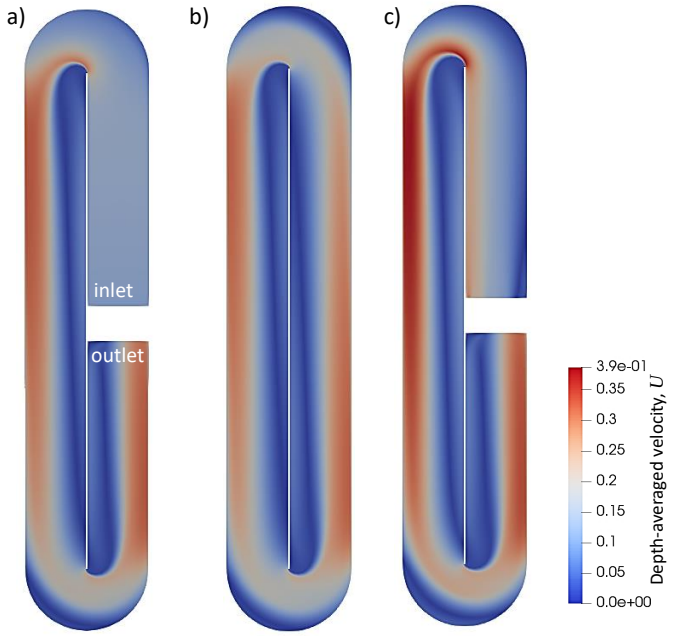

Figure 8: Velocity magnitude contours for a) uniform inlet velocity, b) constant momentum source, and c) non-uniform inlet velocity.

a strong gradient with the highest velocities near the external wall in Figure 8.b (momentum source) and near the central divider in Figure 8.c (non-uniform IV). While this region constitutes only about 25% of the total RWP volume in

Figure 8, this effect becomes more pronounced in RWPs where the paddlewheel is positioned near the bend. This is in line with what was mentioned in section 2.4, where the region downstream of the paddlewheel made up half of the total RWP volume.

3.3. Full-scale RWP

Figure 9 shows the transverse distribution of mean depth-averaged velocities measured at cross-sections located 1.5 m upstream and 2.0 m dowsntream of the paddlewheel axis in a field installation. In this installation, the paddlewheel is positioned at the exit of a bend, and therefore, the distribution of flow velocities impinging on the paddlewheel are substantially different from that observed previously in the laboratory (Section 3.1). Namely the flow velocity has a strong lateral (i.e. $y-$component) component, and the highest magnitudes impinging on the paddlewheel are located close to the central divider. Nonetheless, it is also observed that the paddlewheel induces a remarkable change in the distribution of the depth-averaged velocity. The direction of the approach flow changes significantly from upstream to downstream. The approach flow is characterised by a jet directed towards the outer wall (induced by the flow separation at the bend), which then exits the paddlewheel towards the central divider. The explanation for this phenomenon may be drawn via the same hypothesis invoked for the inversion in streamwise component of the velocity observed in the laboratory. In this case, the transverse component of the approach flow velocity (which is not negligible here) must vanish at the blades and at the outer wall; this deceleration of the transverse component of the velocity gives raise to a lateral pressure gradient, which is responsible for the change in flow direction at the exit of the paddlewheel. The substantial change in the distribution of flow induced by the paddlewheel observed here provides further evidence that approaches commonly used by CFD modellers (i.e. uniform IV or momentum source) are unlikely to accurately model the flow conditions in the vicinity and downstream from paddlewheels.

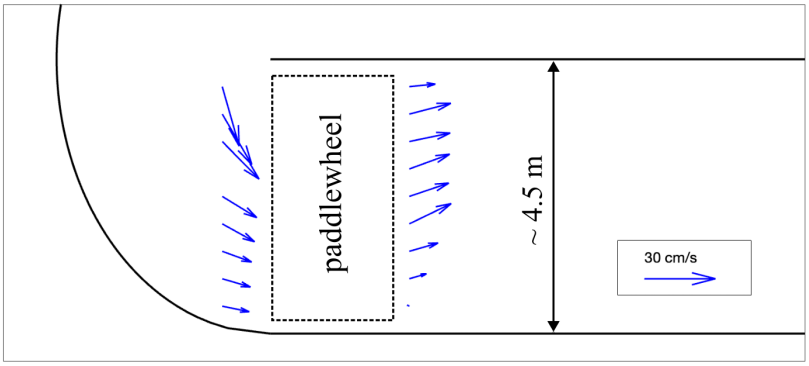

Figure 9: Measured depth-average velocities at cross-sections upstream and downstream of a paddlewheel in a field installation.

4. Conclusions

This work analyses flow in RWPs through an exhaustive set of velocity measurements undertaken using PIV in a laboratory model, along with a set of field measurements conducted in a full-scale RWP. The results from these experiments showed that the spanwise distribution of depth-averaged streamwise flow velocity is substantially altered by the paddlewheel. Namely, laboratory results showed that the flow approaches the paddlewheel with the highest velocities located in the region near the external wall of the RWP, while the flow downstream from the paddlewheel displays the highest velocities on the opposite side of the channel (i.e. a complete inversion of the velocity gradient takes place). A hypothesis was proposed to explain this phenomenon. A substantial change in velocity distribution was also observed in the full-scale installation where the paddlewheel was located immediately downstream of a bend in the RWP. The non-uniform distribution of velocities measured in the laboratory model was then used as the inlet velocity boundary condition of a CFD model to assess the effect of commonly used modelling assumptions on the accuracy of CFD predictions. In particular, the non-uniform IV method, which provided excellent agreement against measured data, was compared against the uniform IV and the momentum source methods, which are widely used in simulations

of flow in RWPs. The results of our comparative analysis shows that such assumptions may lead to substantially inaccurate model predictions of flow between the paddlewheel and the subsequent bend. Errors in model predictions induced by such approaches may have important implications for the design of efficient algae cultivation systems, particularly in RWPs where the paddlewheel is positioned near the bend, and the region downstream of the bend constitutes almost half of the RWP. It is recommended that conclusions previously derived from CFD simulations which might have inaccurately represented the boundary conditions should be revisited.

This research highlights the importance of accurate boundary conditions in CFD simulations of flow in RWPs and provides a foundation for further studies to improve the efficiency of large-scale algae production.

Acknowledgement

The authors acknowledge the support from the Innovate UK through Grant agreement (TS/V002414/1). The authors acknowledge the use of the IRIDIS High Performance Computing Facility, and associated support services at the University of Southampton, in the completion of this work.

References

[1] P. Spolaore, C. Joannis-Cassan, E. Duran, A. Isambert, Commercial applications of microalgae, Journal of bioscience and bioengineering 101 (2) (2006) 87–96.

[2] S. Mobin, F. Alam, Some promising microalgal species for commercial applications: a review, Energy Procedia 110 (2017) 510–517.

[3] A. Demirbas, Use of algae as biofuel sources, Energy conversion and management 51 (12) (2010) 2738–2749.

[4] R. Rajkumar, Z. Yaakob, M. S. Takriff, Potential of micro and macro algae for biofuel production: a brief review, Bioresources 9 (1) (2014) 1606–1633.

[5] R. Bhateria, R. Dhaka, Algae as biofuel, Biofuels 5 (6) (2014) 607–631.

[6] D. J. Gilmour, Microalgae for biofuel production, Advances in applied microbiology 109 (2019) 1–30.

[7] S. Paul, S. Bera, R. Dasgupta, S. Mondal, S. Roy, Review on the recent structural advances in open and closed systems for carbon capture through algae, Energy Nexus 4 (2021) 100032.

[8] R. Sayre, Microalgae: the potential for carbon capture, Bioscience 60 (9) (2010) 722–727.

[9] A. H. Alami, S. Alasad, M. Ali, M. Alshamsi, Investigating algae for co2 capture and accumulation and simultaneous production of biomass for biodiesel production, Science of the Total Environment 759 (2021) 143529.

[10] S. Banerjee, S. Ramaswamy, Dynamic process model and economic analysis of microalgae cultivation in open raceway ponds, Algal research 26 (2017) 330–340.

[11] K. Kumar, S. K. Mishra, A. Shrivastav, M. S. Park, J.-W. Yang, Recent trends in the mass cultivation of algae in raceway ponds, Renewable and Sustainable Energy Reviews 51 (2015) 875–885.

[12] H. Hadiyanto, S. Elmore, T. Van Gerven, A. Stankiewicz, Hydrodynamic evaluations in high rate algae pond (hrap) design, Chemical Engineering Journal 217 (2013) 231–239.

[13] R. Hreiz, B. Sialve, J. Morchain, R. Escudié, J.-P. Steyer, P. Guiraud, Experimental and numerical investigation of hydrodynamics in raceway reactors used for algaculture, Chemical Engineering Journal 250 (2014) 230–239.

[14] S. Sawant, S. Gosavi, H. Khadamkar, C. Mathpati, R. Pandit, A. Lali, Energy efficient design of high depth raceway pond using computational fluid dynamics, Renewable Energy 133 (2019) 528–537.

[15] S. Sawant, H. Khadamkar, C. Mathpati, R. Pandit, A. Lali, Computational and experimental studies of high depth algal raceway pond photobioreactor, Renewable energy 118 (2018) 152–159.

[16] C. Inostroza, A. Solimeno, J. García, J. M. Fernández-Sevilla, F. G. Acién, Improvement of real-scale raceway bioreactors for microalgae production using computational fluid dynamics (cfd), Algal Research 54 (2021) 102207.

[17] J. Huang, X. Qu, M. Wan, J. Ying, Y. Li, F. Zhu, J. Wang, G. Shen, J. Chen, W. Li, Investigation on the performance of raceway ponds with internal structures by the means of cfd simulations and experiments, Algal research 10 (2015) 64–71.

[18] H. Amini, A. Hashemisohi, L. Wang, A. Shahbazi, M. Bikdash, K. Dukka, W. Yuan, Numerical and experimental investigation of hydrodynamics and light transfer in open raceway ponds at various algal cell concentrations and medium depths, Chemical Engineering Science 156 (2016) 11–23.

[19] H. Amini, L. Wang, A. Hashemisohi, A. Shahbazi, M. Bikdash, K. Dukka, W. Yuan, An integrated growth kinetics and computational fluid dynamics model for the analysis of algal productivity in open raceway ponds, Computers and Electronics in Agriculture 145 (2018) 363–372.

[20] T. M. Teshome, Computational fluid dynamics application to optimize and evaluate the performance of high rate algal pond system, Ph.D. thesis, Strasbourg (2020).

[21] A. Lima, B. Marinho, T. Morais, Hydrodynamic analysis of flow in raceway ponds for algae cultivation under versatile conditions, Aquaculture International 29 (1) (2021) 19–35.

[22] R. P. M. Moreira, A. C. Reina, P. S. Molina, J. A. S. Pérez, G. L. Puma, Computational fluid dynamics (cfd) modeling of removal of contaminants of emerging concern in solar photo-fenton raceway pond reactors, Chemical Engineering Journal 413 (2021) 127392.

[23] K. Liffman, D. A. Paterson, P. Liovic, P. Bandopadhayay, Comparing the energy efficiency of different high rate algal raceway pond designs using computational fluid dynamics, Chemical Engineering Research and Design 91 (2) (2013) 221–226.

[24] M. Prussi, M. Buffi, D. Casini, D. Chiaramonti, F. Martelli, M. Carnevale, M. R. Tredici, L. Rodolfi, Experimental and numerical investigations of mixing in raceway ponds for algae cultivation, Biomass and bioenergy 67 (2014) 390–400.

[25] Q. Zhang, S. Xue, C. Yan, X. Wu, S. Wen, W. Cong, Installation of flow deflectors and wing baffles to reduce dead zone and enhance flashing light effect in an open raceway pond, Bioresource Technology 198 (2015) 150–156.

[26] H. Ali, T. A. Cheema, C. W. Park, Effect of paddle-wheel pulsating velocity on the hydrodynamic performance of high-rate algal ponds, Journal of Energy Engineering 141 (4) (2015) 04014039.

[27] M. Raffel, C. E. Willert, J. Kompenhans, et al., Particle image velocimetry: a practical guide, Vol. 2, Springer, 1998.

[28] H. G. Weller, G. Tabor, H. Jasak, C. Fureby, A tensorial approach to computational continuum mechanics using object-oriented techniques, Computers in physics 12 (6) (1998) 620–631.

[29] J. Boussinesq, Essai sur la théorie des eaux courantes, Impr. nationale, 1877.

[30] B. E. Launder, B. I. Sharma, Application of the energy-dissipation model of turbulence to the calculation of flow near a spinning disc, Letters in heat and mass transfer 1 (2) (1974) 131–137.